Materials Horizons

Photo-Controllable Microcleaner: Photo-Induced Crawling Motion and Particle Transport of Azobenzene Crystals on a Liquid-Like Surface

Journal:	*Materials Horizons*
Manuscript ID	MH-COM-04-2024-000455.R1
Article Type:	Communication
Date Submitted by the Author:	24-Jun-2024
Complete List of Authors:	Saikawa, Makoto; University of Tsukuba; National Institute of Advanced Industrial Science and Technology Tsukuba Center Tsukuba Central Ohnuma, Mio; National Institute of Advanced Industrial Science and Technology Tsukuba Center Tsukuba Central Manabe, Kengo; National Institute of Advanced Industrial Science and Technology Tsukuba Center Tsukuba Central, Research Institute for Advanced Electronics and Photonics Saito, Koichiro; National Institute of Advanced Industrial Science and Technology Tsukuba Center Tsukuba Central, Electronics and Photonics Research Institute Kikkawa, Yoshihiro; National Institute of Advanced Industrial Science and Technology Tsukuba Center Tsukuba Central Norikane, Yasuo; National Institute of Advanced Industrial Science and Technology Tsukuba Center Tsukuba Central,

Photo-Controllable Microcleaner: Photo-Induced Crawling Motion and Particle Transport of Azobenzene Crystals on a Liquid-Like Surface

Makoto Saikawa, Mio Ohnuma, Kengo Manabe, Koichiro Saito, Yoshihiro Kikkawa and Yasuo Norikane

New Concepts

We demonstrate a new concept of “photo-controllable microcleaner” using the crawling motion of photoresponsive organic crystals. Unlike conventional soft actuators based on elastomers or composites, the microcleaner is a single-component transporter, eliminating the need to mix, mold, and assemble components. The microcleaner can capture and carry microparticles on a solid surface, and even change the direction of transport without releasing the particles. Sublimation, a property unique to crystals, allows the microcleaner to release the particles. Furthermore, simple irradiation with commercial LEDs simultaneously controls multiple crystals as microcleaners, and each microcleaner can handle multiple microparticles at the same time. The finding of this study opens up great potential for the development of novel techniques in soft robotics and microfluidics.

COMMUNICATION

Photo-Controllable Microcleaner: Photo-Induced Crawling Motion and Particle Transport of Azobenzene Crystals on a Liquid-Like Surface

Received 00th January 20xx,
Accepted 00th January 20xx

DOI: 10.1039/x0xx00000x

Makoto Saikawa,[ab] Mio Ohnuma,[b] Kengo Manabe,[b] Koichiro Saito,[b] Yoshihiro Kikkawa [b] and Yasuo Norikane*[bc]

Organic crystals of 3,3'-dimethylazobenzene (DMAB) exhibit photo-induced crawling motion on solid surfaces when they are simultaneously irradiated with ultraviolet and visible light from opposite directions. DMAB crystals are candidates for light-driven cargo transporters having simple chemical compositions and material structures. However, fast crawling motion without significant shape deformation has not yet been achieved. In this study, compared with hydrophilic glass and conventional hydrophobic surfaces with alkyl chains, siloxane-based hybrid surfaces, which are "liquid-like surfaces," result in the fastest crawling motion (4.2 μm min^{-1}) while a droplet-like shape of DMAB crystals is maintained. Additionally, we successfully demonstrate that the DMAB crystals are capable of capturing and carrying silica particles on the hybrid surface. The transport direction is changed on demand without releasing the particles by simply changing the irradiation direction. The particles can be left on the substrate by removing the DMAB crystals via sublimation at room temperature. This result showcases a new concept of "photo-controllable microcleaner" that can operate a series of cargo capture–carry–release tasks. We expect this transporter to contribute to the development of crystal actuators, microfluidics, and microscale molecular flasks/reactors.

Introduction

Soft actuators, which are organic materials that exhibit stimuli-responsive actuations,[1] are promising materials for diverse applications such as soft robotics,[2–4] flexible electronics,[5–7] and biomedical applications[8–10] because they offer high flexibility and adaptability and are lightweight in contrast to conventional hard actuators.[11] Light is a particularly attractive stimulus because it is contactless, spatiotemporally controllable, and environmentally friendly.[12] Sunlight, which is an inexhaustible source of energy, can be used to trigger motion.[13] Therefore, advances in light-driven actuators would contribute to sustainable development. Various organic materials that exhibit light-driven actuation and are based on liquid-crystal polymers,[14–16] composites,[17–21] amorphous materials,[22–24] and crystals[25,26] have been reported.

Actuator materials based on organic crystals have attracted considerable attention. Because organic molecules are packed in an orderly manner in crystals, microscopic structural changes, such as isomerization and dimerization, can be amplified into macroscopic actuation. Compared with polymer materials, the simplicity of the chemical components and structures facilitates a discussion on the relationship between the molecular structure and actuation properties.[27,28] To date, various photo-induced crystal motions have been reported.[25,26] Those motions have been applied to perform tasks,[29] such as displacing an object,[30–32] lifting an object,[32–38] rotating a gearwheel,[38] manipulating a micro-particle,[39,40] trapping nanoparticles,[41] switching an electric circuit ON/OFF,[42] and releasing encapsulated contents.[43–45] However, only the bending or breaking (salient) motion of crystals has been applied in previous studies. Therefore, research on the application of other crystal motions to perform tasks is ongoing.

The photo-induced crawling motion of crystals is one candidate for performing tasks. Crystals of azobenzene derivatives exhibit this motion on solid surfaces under light irradiation.[46,47] The crystals of *trans*-3,3'-dimethylazobenzene (DMAB) (Fig. 1a) move when simultaneously irradiated with ultraviolet (UV) (365 nm) and visible (465 nm) light from opposite directions (Fig. 1b).[46] UV light induces photoisomerization from a *trans* to *cis* isomer, resulting in melting of the crystals (photomelting). Visible light induces a

[a] Graduate School of Science and Technology, University of Tsukuba, Tsukuba, Ibaraki 305-8571, Japan
[b] Research Institute for Advanced Electronics and Photonics, National Institute of Advanced Industrial Science and Technology (AIST), Tsukuba, Ibaraki 305-8565, Japan. E-mail: y-norikane@aist.go.jp
[c] Faculty of Pure and Applied Sciences, University of Tsukuba, Tsukuba, Ibaraki 305-8571, Japan

† Electronic Supplementary Information (ESI) available. See DOI: 10.1039/x0xx00000x

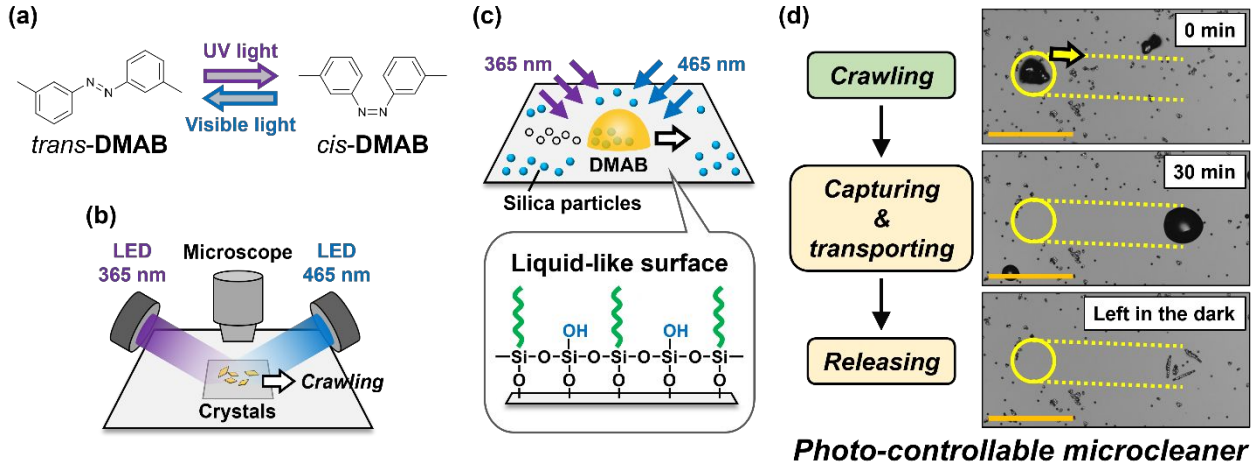

Fig. 1 (a) Chemical structure and photoisomerization of DMAB. (b) Schematic illustration of the experimental setup for observing the crawling motion of DMAB crystals. (c) Schematic illustration of the transport of silica particles and siloxane-based liquid-like surface. (d) Photomicrographs of the crawling motion of DMAB crystals performing a series of capture–carry–release tasks of silica particles having a diameter of 2 μm. Scale bar: 100 μm.

reverse reaction from a *cis* to *trans* isomer, which contributes to the recrystallization of the crystal. Crystals of *trans*-4-(methylamino)azobenzene (MAAB) also exhibit the crawling motion when irradiated with a single light source to induce photomelting because of a fast thermally induced *cis*-to-*trans* reaction.[47] For both cases, the nonequilibrium state with photomelting and recrystallization in the crystals is considered to be the driving force for their crawling motion. The mechanism of the crawling motion was discussed in detail in our previous paper.[48] Notably, their motions are phototactic. The crystals of both these materials move away from the light source inducing photomelting. Therefore, the direction of light irradiation determines the direction of travel. The crystal-crawling system has an additional advantage. Multiple crystals continue crawling when the entire substrate is simply illuminated with light-emitting diodes (LEDs). In contrast, other soft actuators often require precise light manipulation or tracking to maintain motion.[28,49,50]

To induce the crawling motion of DMAB or MAAB crystals, a photomelting process is necessary. Thus, the crystals are expected to capture the target cargo and transport it. Our group recently reported that MAAB crystals successfully transport nanoparticles on a glass substrate.[51] However, the nanoparticles were premixed with crystals before the transport. To the best of our knowledge, no studies on organic crystals successfully performing a series of cargo capture–carry–release tasks have been conducted. Demonstrations of azobenzene crystals performing multiple tasks would provide novel application possibilities for crystal actuators: a new method for small-scale manipulation used in, for example, microfluidics and particle assembly.

Our previous studies revealed that the moving velocity and shape of DMAB crystals strongly depend on surface properties such as hydrophilicity or hydrophobicity.[48,52] Both rapid movements and shape maintenance are considered to be impotant for the crawling crystal to be applied to a transporter. However, these two aspects have not yet been combined. In our aforementioned previous studies, the crystals showed significant shape deformation on hydrophilic surfaces, while they maintained a droplet-like shape but moved much slower on hydrophobic surfaces.

Because the crawling motion of DMAB crystals is strongly affected by the surface, we focused on optimizing the motion by controlling the surface properties. Numerous types of surface modifications have been designed to control the wettability of droplets on substrate surfaces.[53–56] Several indices such as the contact angle, surface free energy, and roughness are used to evaluate the surface and discuss droplet behavior on the surface. Static contact angle (θ_S) is widely used to quantify the wettability of a droplet on a substrate. In this study, we paid particular attention to the contact angle hysteresis ($\Delta\theta_{cos}$), which is defined as $\Delta\theta_{cos} = \cos\theta_{Rec} - \cos\theta_{Adv}$, where θ_{Adv} and θ_{Rec} are the advancing and receding contact angles, respectively. The contact angle hysteresis is an indication of removability of a droplet from the substrate: how little force is required for a droplet to slide off the substrate surface.[57] Because DMAB crystals are considered to be partially liquefied during crawling, they are expected to behave similar to liquids. Therefore, we hypothesize that selecting a surface based on $\Delta\theta_{cos}$, which is typically used to evaluate the slipperiness of droplets, is possible to control the moving velocity and the shape of the crystals during the motion.

"Liquid-like surfaces" have the notable characteristic of an extremely small $\Delta\theta_{cos}$.[58,59] The high flexibility and mobility of surface-tethered functional groups endow these surfaces with a liquid-like nature, which results in droplets sliding off easily and a small $\Delta\theta_{cos}$. Various approaches, such as optimizing the chain length,[60] reducing the crosslinking degree,[61] and reducing the packing density,[62,63] have been proposed to achieve the high flexibility and mobility of surface-tethered functional groups. In addition, liquid-like surfaces are generally hydrophobic. Because crawling DMAB crystals display a droplet-like shape on hydrophobic surfaces, they are anticipated to move rapidly and maintain their shape on hydrophobic liquid-like surfaces.

Here, we aimed to achieve the highest velocity of the crawling motion of DMAB crystals without significant shape deformation and apply this motion to transport the target cargo. First, we investigated the crawling motion of crystals on siloxane-based hybrid surfaces, which are "liquid-like surfaces." (Fig. 1c). The crystals moved the fastest on these surfaces (~4.2 μm min^{-1}) compared with on hydrophilic glass (3.3 μm min^{-1} [48]) and conventional hydrophobic surfaces with alkyl chains (~2.5 μm min^{-1}). The crystals maintained a droplet-like shape during the crawling motion on the hybrid surfaces. The small $\Delta\theta_{cos}$ and hydrophobicity of the hybrid surfaces contributed to achieving both the highest velocity and maintaining the shape. Second, we attempted to utilize the crawling motion to perform a series of capture–carry–release tasks for silica particles (Fig. 1c and 1d). This novel function of organic crystals was successfully achieved using DMAB crystals on only the hybrid surface. This result provides a new concept of "photo-controllable microcleaner" on a solid surface.

Results and discussion

Preparation of substrates

Hozumi et al. prepared siloxane-based hybrid films using alkyltriethoxysilanes and tetramethoxysilane (TMOS).[62,63] The surfaces of the hybrid films exhibited a liquid-like nature due to silanol groups derived from TMOS, which provided sufficient space for the alkyl groups to rotate or move freely, resulting in a small $\Delta\theta_{cos}$ of the surface. In this study, hybrid films with C_3, C_6, C_{10}, and C_{16} for the alkyl chain length were prepared as per the literature[63] and referred to as Hyb3, Hyb6, Hyb10, and Hyb16, respectively. Each film was obtained by spin-casting and subsequent drying of each precursor solution on a glass substrate at 25 °C in air. For control experiments, hydrophilic glass, and conventional hydrophobic films with alkyl chain lengths of C_{10}, C_{16}, and fluorinated C_{10} were prepared without TMOS (referred to as TMS10, TMS16, and FAS10, respectively), as per the literature.[48]

All films, except the Hyb16 film, were colorless and transparent; the Hyb16 film was colorless but opaque. This finding was consistent with literature results and could be attributed to the higher surface roughness of the Hyb16 film.[63] The surface roughness was evaluated by measuring the root-mean-square roughness (R_{rms}) using atomic force microscopy (AFM) in a scan area of 3 × 3 μm^2 as reported in the literature[63] (Fig. S1, ESI†). The R_{rms} of the Hyb16 film was found to be significantly higher (>30 nm) than those of the other films (0.32–0.54 nm).

To compare the surface wettability of the films, the θ_s, θ_{Adv}, θ_{Rec}, and sliding angle (θ_α) of a water droplet were measured, and $\Delta\theta_{cos}$ was calculated (Table S1 and Fig. S2, ESI†). The hybrid surfaces (Hyb3, Hyb6, Hyb10, and Hyb16) and the conventional hydrophobic surfaces (TMS10, TMS16, and FAS10) exhibited comparable hydrophobicity (θ_s); however, the hybrid surfaces had smaller θ_α and $\Delta\theta_{cos}$ than the hydrophobic surfaces. Thus, the hybrid surfaces were confirmed to be liquid-like surfaces. The contact and sliding angles were measured using melted DMAB at room temperature instead of water as the probe liquid

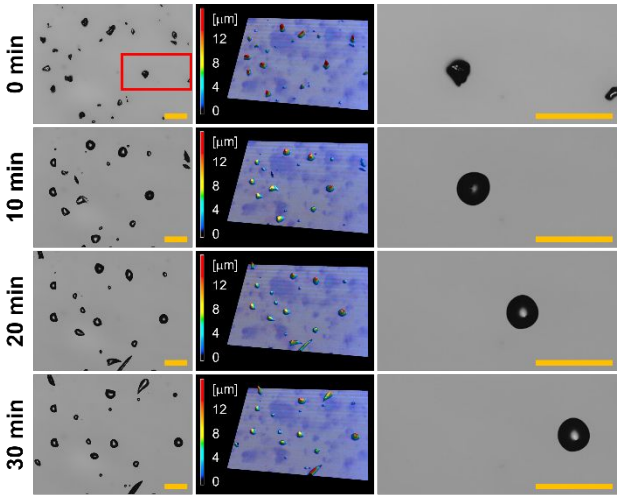

Fig. 2 Photomicrographs of the crawling motion of DMAB crystals on the Hyb10 film after irradiation for t = 0, 10, 20, and 30 min. The first column presents the photomicrographs of the entire field of view, second column shows 3D images obtained by using a laser scanning microscope, and third column depicts enlarged images of the square in the first column. Light irradiation was performed from the left for UV (365 nm) light and from the right for visible (465 nm) light. The intensities of 365 and 465 nm were 200 and 50 mW cm^{-2}, respectively. Scale bar: 100 μm.

(Table S2 and Fig. S2, ESI†). The melting points of DMAB were 53 °C and 43–46 °C for *trans* and *cis* isomers, respectively;[46] however, the droplets of *trans*-DMAB obtained at 60 °C did not recrystallize immediately at room temperature as long as they were handled gently owing to a supercooled state. The values obtained by using water and melted DMAB exhibited similar trends (Fig. S3, ESI†). The details are discussed later.

Crawling motion

The crawling experiments on DMAB crystals on the hybrid surfaces (liquid-like surfaces) were performed as described in our previous reports.[48,52] Polycrystals of *trans*-DMAB were ground using a mortar and pestle and placed randomly on the substrate through a 25 μm mesh. The crystals were exposed to UV (365 nm) and visible (465 nm) light at intensities of 200 and 50 mW cm^{-2}, respectively. The irradiation light intensities were optimized to observe the crawling motion in our previous work.[46] The photomicrographs of the DMAB crystals on the Hyb10 film during exposure are shown in Fig. 2. After 30 min of exposure, almost all crystals in the field of view moved away from the UV light source (ESI,† Movie S1). This indicated that the DMAB crystals exhibit photo-induced crawling motion on liquid-like surfaces, as observed in our previous studies.[46,48,52] Notably, the crystals displayed a droplet-like shape after irradiation and maintained this shape during movement (Fig. 3). The shape of the crystals during movement is discussed later. The total travel distance for 30 min was distributed (Fig. S4a, ESI†), with some DMABs stopping during light irradiation. On average, the crystals traveled 99±55 μm in 30 min on the Hyb10 film. When the moving DMAB was assumed to a spherical segment with a bottom diameter of 40 μm (Fig. 3), the crystals

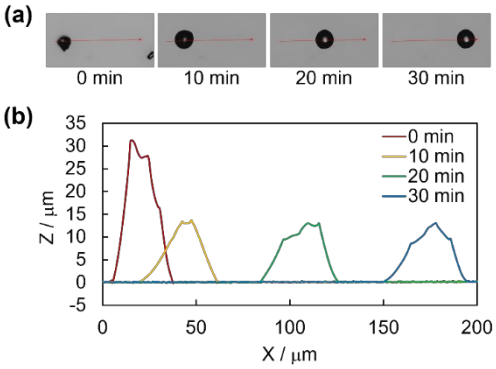

Fig. 3 Height profiles of crawling DMAB crystals on the Hyb10 film observed by using laser confocal microscope. (a) Photomicrographs of DMAB crystals on the Hyb10 film after irradiation for t = 0, 10, 20, and 30 min. (b) Height profiles of the DMAB crystals along the red arrow in (a) after irradiation for t = 0, 10, 20, and 30 min.

moved approximately 2.5 times their own size in 30 min. The avarage moving velocity was calculated to be 4.2±1.7 μm min^{-1} (Fig. S4b, ESI†), which is the highest velocity compared with results of our previous studies.[46,48,52]

Although crawling DMAB appeared as a droplet, a single droplet was considered to be a mixture of crystals and liquid. Polarized optical microscopy revealed birefringence in crawling DMAB (Fig. 4). The birefringence disappeared upon irradiation with only UV light (Fig. S5, ESI†). Therefore, the birefringence observed in crawling DMAB was considered to originate from the crystals. Other experiments strongly supported the existence of crystals in crawling DMAB (Fig. S6–S8 and their description, ESI†). In the case of an individual DMAB, a comparison between the image without the polarizer and that under the crossed-polarizer orientation in Fig. 4 revealed that the latter had a smaller area. The difference between their areas clearly indicated that the entire crawling DMAB was not fully crystalline but partially liquid. Although quantifying the volume ratio of crystal/liquid is not currently possible, the presence of the mixture is essential for inducing the crawling motion. These observations support the hypothesis that moving DMABs can capture and carry the target cargo.

The photo-induced crawling motion of DMAB crystals was also observed on the Hyb3, Hyb6, and Hyb16 films (Fig. S9–S11, Movie S2–S4, ESI†). For each substrate, a droplet-like shape was maintained during movement, similar to the results obtained for the Hyb10 film (Fig. S14–S16, ESI†). The alkyl chain length affected the average travel distance and average velocity (Fig. S4, ESI†). The average moving velocities on Hyb6 (4.2±1.9 μm min^{-1}) and Hyb10 (4.2±1.7 μm min^{-1}) were equivalent and higher than those on Hyb3 (3.7±1.8 μm min^{-1}) and Hyb16 (2.0±1.3 μm min^{-1}). Although DMAB crystals moved on the conventional hydrophobic surfaces of TMS10 (2.5±1.5 μm min^{-1}) and TMS16 (1.8±1.1 μm min^{-1}) (Fig. S12 and S13, Movie S5 and S6, ESI†), the moving velocities on Hyb3, Hyb6, and Hyb10 were found to be considerably higher. On all surfaces tested in this work, the crystals moved faster than on the previously reported FAS10 (0.3 μm min^{-1} [48]).

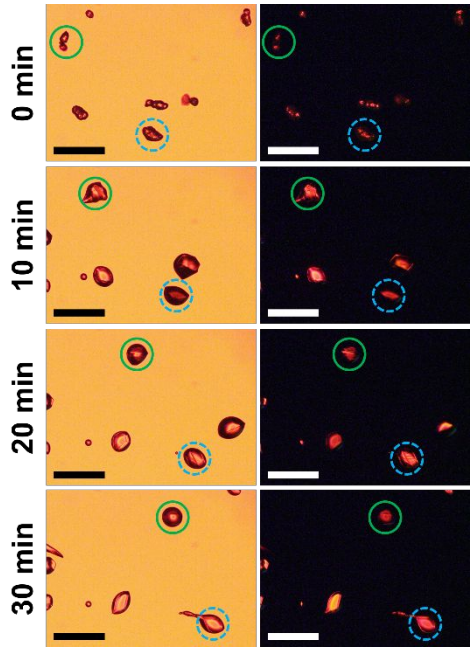

Fig. 4 Photomicrographs of the crawling motion of DMAB crystals on the Hyb10 film after irradiation for t = 0, 10, 20, and 30 min. The first column presents photomicrographs under bright-field, and the second column shows photomicrographs under polarizing optical microscopes with crossed-polarizer orientation. Light irradiation was performed from the left for UV (365 nm) light and from the right for visible (465 nm) light. The intensities of 365 and 465 nm were 200 and 50 mW cm^{-2}, respectively. Colored circles are used to easily see identical crystals. Scale bar: 100 μm.

Correlation between moving velocity and $\Delta\theta_{cos}$

To investigate the correlation between the moving velocity and $\Delta\theta_{cos}$ for various surfaces, the average velocity was plotted against $\Delta\theta_{cos}$ (Fig. 5). A negative correlation existed between the velocity and $\Delta\theta_{cos}$ except for Hyb16 and hydrophilic glass surfaces (correlation coefficient (r) = −0.99; Fig. S21a, ESI†). The $\Delta\theta_{cos}$ was calculated to be 0.15 for Hyb3, 0.12 for Hyb6, 0.09 for Hyb10, and 0.09 for Hyb16. The $\Delta\theta_{cos}$ was 0.21, 0.24, and 0.36 for TMS10, TMS16, and FAS10, respectively (which were the conventional hydrophobic surfaces used as control experiments). Hyb3, Hyb6, and Hyb10 showed smaller $\Delta\theta_{cos}$ and higher moving velocities than the conventional alkyl chain surfaces (Fig. 5). Among the three liquid-like surfaces, Hyb6 and Hyb10 showed relatively smaller $\Delta\theta_{cos}$ and higher velocities than Hyb3. These results indicated that the moving velocity tended to increase with a decreasing $\Delta\theta_{cos}$ of the surface. When the velocity was plotted against θ_α instead of $\Delta\theta_{cos}$ as an indicator of droplet slipperiness, a similar negative correlation was observed (r = −0.99; Fig. S19 and S21c, ESI†).

We also plotted the average velocity against $\Delta\theta_{cos}$' or θ_α', which were measured using melted DMAB as the probe liquid (Fig. S20 and S21, ESI†). Contrary to expectations, a weaker negative correlation was observed compared with that

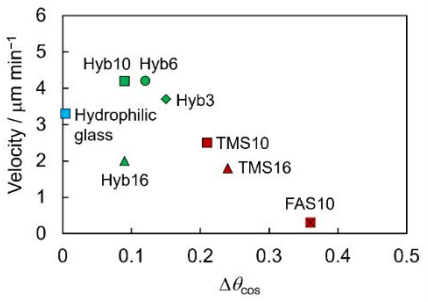

Fig. 5 Plots of the moving velocity of DMAB crystals against the contact angle hysteresis ($\Delta\theta_{cos}$). Probe liquid: water (10 μL).

observed in Fig. 5 and S19; the *r* values, except for Hyb16 and hydrophlic glass, were −0.76 and −0.74 against $\Delta\theta_{cos}$' and θ_{α}', respectively. The substrate wettability was evaluated equally well with water and melted DMAB (Fig. S3, ESI†). Notably, a relatively good correlation was observed in the plots of the sliding angle (r = −0.81) and contact angle hysteresis (r = −0.89). Thus, the correlation efficients using θ_{α} or $\Delta\theta_{cos}$ measured with water or θ_{α}' or $\Delta\theta_{cos}$' measured with melted DMAB should have been similar. However, a considerable difference in the correlation coefficients was observed because of two possible reasons. First, because crawling DMAB contains crystals of a *trans* isomer, as mentioned earlier, it might not behave as a pure liquid. Second, crawling DMAB is a mixture of *trans* and *cis* isomers. Because the thermally melted DMAB used to measure the contact angle consists only of the *trans* isomer, it is unlikely to exhibit the same properties as crawling DMAB, which contains both *trans* and *cis* isomers with different polarities. Thus, the correlation between the moving velocity and $\Delta\theta_{cos}$ or θ_{α} was higher when water was used as the probe liquid in this system.

Although the $\Delta\theta_{cos}$ of the Hyb16 film was comparable to those of the Hyb6 and Hyb10 films, the average moving velocity on the Hyb16 film was much lower than those on the others (Fig. 5). This disparity may be attributed to the substantially higher R_{rms} of the Hyb16 film compared with those of the other surfaces, as mentioned above. The large microscopic surface roughness may have hindered the crawling motion. Despite the larger R_{rms}, $\Delta\theta_{cos}$ was still small for the Hyb16 film, which may be attributed to the differences in the volume of DMAB used for each measurement. Although 10 μL of water or 3 μL of melted DMAB was used to measure the contact and sliding angles, the DMAB crystals used in the crawling experiments were those that passed through a 25 μm mesh sieve. The volume of the crawling crystal was roughly estimated to be 6.8×10^3 μm^3 (6.8×10^{-6} μL), assuming a spherical segment having a bottom radius of 20 μm and a height of 10 μm (Fig. 3). Consequently, the crawling motion was considered to be strongly affected by microscopic surface roughness. Therefore, accurately predicting the velocity solely based on $\Delta\theta_{cos}$ may not be possible, but it can still be a useful value if the surface is smooth enough.

The hydrophilic glass surface had the smallest $\Delta\theta_{cos}$ (0.004 for water) among the surfaces examined in this study. However, it did not exhibit the highest moving velocity of DMAB crystals (3.3 μm min^{-1} [48]) (Fig. 5). The reason for this result was not entirely clear but presumed to be the θ_S of the hydrophilic glass surface being the smallest among those of the other surfaces; this allowed the crystals to deform significantly while moving. Because of the difficulty in shrinking the rear side of the crystal, liquefied DMAB (melted by using UV light) may not have been efficiently supplied from the back to the front side of the crystal.[48] As a result, compared with the hybrid surfaces, the hydrophilic glass surface was considered to achieve less effective propulsion away from the UV light source. The smaller $\Delta\theta_{cos}$ was shown to contribute to faster crawling motion as long as θ_S was high, and a smaller $\Delta\theta_{cos}$ can work to some extent even when θ_S was small.

Shape of crystals during crawling motion

The crawling experiments on DMAB crystals on the hybrid surfaces provided invaluable insights into both the moving velocity and the shape of the crystals during movement. As mentioned earlier, the hybrid surfaces (Hyb3, Hyb6, and Hyb10) contributed to a faster crawling motion compared with conventional hydrophobic surfaces with alkyl chains (TMS10, TMS16, and FAS10) and hydrophilic glass surfaces. Furthermore, the crystals exhibited a droplet-like shape while moving on the hybrid surfaces; this was consistent with the results obtained for conventional hydrophobic surfaces (Fig. S17 and S18, ESI†) and previously investigated hydrophobic surfaces.[48,52] This is in considerable contrast to the distinct deformation of the crystals observed on the hydrophilic glass surface.[48] The static contact angles (θ_S) of the hybrid surfaces (88–105°) and conventional hydrophobic surfaces (99–104°) were found to be comparable and much higher than that of the hydrophilic glass surface (10°) (Table S1, Figure S2a, ESI†). Consistent results were obtained when evaluating θ_{Adv} or θ_{Rec} and when using melted DMAB as the probe liquid (Table S1 and S2, Figure S2, ESI†). Although which value among θ_S, θ_{Adv}, or θ_{Rec} was dominant was unclear, a higher contact angle was necessary to maintain the droplet-like shape during crawling.

In our previous studies,[48,52] hydrophilic surfaces were necessary to increase the moving velocity of DMAB crystals, resulting in deformation of the crystals as they moved. However, the hybrid surfaces (Hyb3, Hyb6, and Hyb10) combined excellent slipperiness, owing to the small $\Delta\theta_{cos}$, with high contact angles, which enabled faster movement while the droplet-like shape was maintained. This feature may overcome the trade-off between the high velocity and shape maintenance observed on conventional hydrophobic and hydrophilic surfaces.

Transport of silica particles

DMAB crystals were expected to capture and carry cargo as they moved because their crawling motion was accompanied by the partial photomelting of the crystals, as mentioned above and the literature.[48] In this study, monodispersed and spherical silica particles having diameters of 2, 5, 10, and 20 μm were employed as the target cargo (Fig. S22, ESI†). We preliminarily confirmed that the surfaces of the silica particles had good

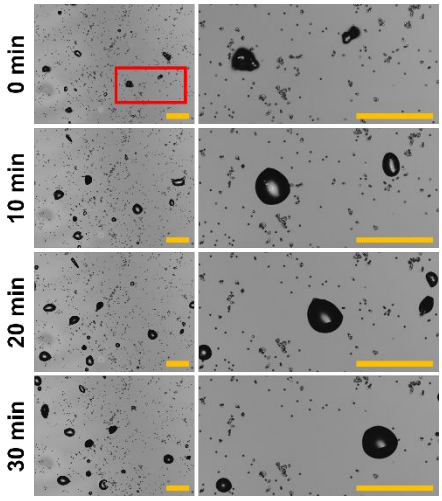

Fig. 6 Photomicrographs of the crawling motion of DMAB crystals on the Hyb10 film where silica particles having a diameter of 2 μm were placed after irradiation for t = 0, 10, 20, and 30 min. The first column presents photomicrographs of the entire field of view, and the second column shows enlarged images of the square in the first column. Light irradiation was performed from the left for UV (365 nm) light and from the right for visible (465 nm) light. The intensities of 365 and 465 nm were 200 and 50 mW cm^{-2}, respectively. Scale bar: 100 μm.

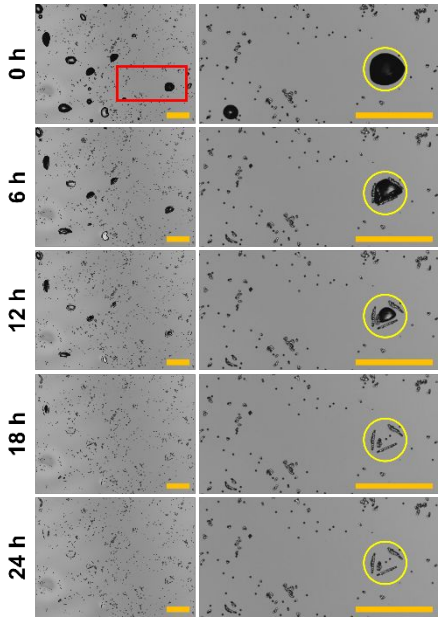

Fig. 7 Photomicrographs of DMAB crystals on the Hyb10 film after transporting silica particles having a diameter of 2 μm depicted in Fig. 6. The sample presented in Figure 6 was left in the dark at 25 °C for t = 0, 6, 12, 18, and 24 h. The first column shows photomicrographs of the entire field of view, and the second column reveals enlarged images of the square in the first column. Scale bar: 100 μm.

wettability against melted DMAB (Fig. S23 and its description, ESI†). This result indicated that the crawling DMABs would continue to hold particles during transport without separation.

The transport of silica particles having a diameter of 2 μm was attempted (Fig. 6 and ESI,† Movie S7). The DMAB crystals and silica particles were not premixed and were placed randomly on the Hyb10 film (0 min) (Fig. 6). The crystals and particles were then exposed to UV and visible light. The crystals continued to move away from the UV light source and maintained a droplet-like shape during the 30 min of exposure. This result is similar to the crawling motion without silica particles (Fig. 2). Surprisingly, no silica particles remained on the path through which the crystals moved. Therefore, the crystals successfully captured and transported the particles. In other words, the crystals cleaned the particles along their path as they moved away from the UV light source. Notably, the DMAB crystals were demonstrated to be a "photo-controllable microcleaner" on the Hyb10 film.

To confirm that an upper limit to the number of particles that could be transported exists, large amounts of silica particles having a diameter of 2 μm were transported on the Hyb10 film (Figure S24 and Movie S8, ESI†). Only crawling motion was observed, and no silica particles were left behind during the first 10 min. However, with further irradiation after 10 min, the crawling DMAB began to lose its shape and carrying the particles became almost impossible. Therefore, too many silica particles seemed to prevent the crawling motion, probably because the particles accumulated at the bottom of the moving DMAB and prevented contact between the moving DMAB and the substrate surface.

The carrying medium was removed from the mixture of DMAB and silica particles after transport via sublimation of the DMAB crystals. After 30 min of transporting silica particles having a diameter of 2 μm, the mixture of DMAB and silica particles was left in the dark at room temperature (Fig. 7). Notably, the crystal mass gradually decreased. After 24 h in the dark, all the crystals in the entire field of view disappeared, and only silica particles remained on the substrate. Therefore, DMAB crystals could release silica particles after transport if they are simply left in the dark. Thus, DMAB crystals could deliver cargo to targeted locations because of remote manipulation with light. To the best of our knowledge, this is the first example of an organic crystal that successfully performs a series of cargo capture–carry–release tasks.

The effect of the silica particle size was investigated using large silica particles on the Hyb10 film. The DMAB crystals successfully transported silica particles having diameters of 5 and 10 μm while maintaining a droplet-like shape (Fig. S25 and S26, Movie S9 and S10, ESI†). However, transport was unsuccessful for particles having a diameter of 20 μm (Fig. S27 and Movie S11, ESI†). In this case, the DMAB crystals and silica particles coalesced but barely moved. This size limitation might be due to the height of the crawling DMAB crystals. Because the height of the crystals during movement was approximately 10 μm (Fig. 3), silica particles having a diameter of 20 μm were extremely large for transport. Another possible reason for the unsuccessful transport is that silica particles having a diameter of 20 μm were immensely heavy. The critical properties of the

particles, such as material, size, density, and wettability with DMAB, which are important for transport, are currently being investigated.

As a control experiment, the transport of silica particles having a diameter of 2 μm was attempted on hydrophilic glass and the TMS10 film. Transport was unsuccessful on both surfaces. On hydrophilic glass, the deforming crystals that captured the particles appeared to split as they moved (Fig. S28 and Movie S12, ESI†). On the TMS10 film, the crystals significantly deformed and spread as they moved. Consequently, capturing and carrying the particles were less efficient on these surfaces than those on the Hyb10 film (Fig. S29 and Movie S13, ESI†). Thus, the hybrid surface was found to be more suitable for achieving an object transport system using the crawling motion of DMAB.

"Zigzag" crawling and transport

As previously mentioned, DMAB crystals move away from a UV light source and toward a visible light source. Taking advantage of this phototactic feature, we controlled the direction of movement on the Hyb10 film. Two sets of orthogonally aligned light sources at 365 and 465 nm were prepared, and the DMAB crystals were alternately exposed to each pair of light sources (Fig. S30, ESI†). The first set was designed to move from left to right (Direction A), and the second set was designed to move from front to back (Direction B). During the experiments, the direction was changed twice. The pair of lights switched on was changed every 20 min. As expected, the crystals moved in a zigzag manner (Fig. S31 and Movie S14, ESI†). Based on these results, we added silica particles having a diameter of 2 μm. The zigzag movement was successfully demonstrated along with the capturing and carrying of silica particles (Fig. 8 and ESI,† Movie S15). The crystals continued to transport the silica particles without releasing them even when they changed their direction of movement. The droplet-like shape did not collapse during transport. Therefore, the movement direction of the "photo-controllable microcleaner" could be changed by changing the direction of light irradiation.

Although several studies have been conducted on light-driven solid transport on a substrate by crystals,[51] polymers,[64,65] and droplets,[66,67] materials that perform a series of cargo capture–carry–release tasks are very limited.[68] Multitasking on a substrate remains challenging because the exact opposite actions, capture and release, should be performed with the same material before and after transport. To overcome this difficulty, a soft robot[68] was assembled using different photoresponsive polymer films. Note that the DMAB crystals, as single-component transporters, achieved multitasking on the hybrid surface without assembly. In addition, each DMAB crystal transported several particles simultaneously by capturing the particles while moving rather than handling each particle individually. We expect these advantages to be crucial for further applications of this crystal transporter in microfluidics, microscale molecular flasks/reactors, and particle assembly in terms of efficient transport and reaction.

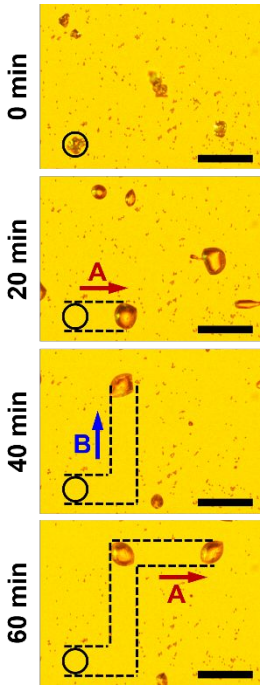

Fig. 8 Photomicrographs of the "zigzag" crawling motion of DMAB crystals on the Hyb10 film where silica particles having a diameter of 2 μm were placed after irradiation for t = 0, 20, 40, and 60 min. The 1st irradiation (0–20 min) and 3rd irradiation (40–60 min) was performed from the left for UV (365 nm) light and from the right for visible (465 nm) light. The 2nd light irradiation (20–40 min) was performed from the bottom for UV (365 nm) light and from the top for visible (465 nm) light. The intensities of 365 and 465 nm were 200 and 50 mW cm^{-2}, respectively. The arrows and letters (A or B) in the photomicrographs indicate the direction in which the DMAB crystals were moving. Scale bar: 100 μm.

Conclusions

Using siloxane-based hybrid surfaces, which are liquid-like surfaces, we achieved the highest velocity (4.2±1.7 μm min^{-1}) of the crawling motion of DMAB crystals and successfully applied this motion to transport a target cargo. The droplet-like shape of crawling DMAB was maintained on the hybrid surfaces, in contrast to on the hydrophilic surface. Owing to the small $\Delta\theta_{cos}$ and hydrophobicity of the hybrid surfaces, both the highest velocity and shape maintenance were achieved. When hydrophilic and conventional hydrophobic surfaces are employed, achieving both the aforementioned features requires a trade-off. In addition, the DMAB crystals successfully captured and transported silica particles while crawling and released them on the hybrid surface via sublimation. To the best of our knowledge, this is the first example of an organic crystal that successfully performs multiple tasks of cargo capture, carry, and release. Thus, we proposed a new concept of a "photo-controllable microcleaner." Multitasking can be performed on a surface that is easily fabricated and flat and lacks flow paths. These results highlight the potential of photo-induced crawling crystals in microfluidics, microscale molecular

flasks/reactors, and methods for particle assembly. Research on these interesting applications using crawling crystals is in progress.

Author Contributions

M.S. conducted the experiments and drafted the manuscript; M.O., K.M., K.S., and Y.K. helped with the analysis of the data; K.M. helped with the preparation of the substrates; Y.N. guided the work and drafted the manuscript. All authors contributed to the discussion and preparation of the manuscript. All authors have given approval to the final version of the manuscript.

Conflicts of interest

There are no conflicts to declare.

Acknowledgements

This work was supported by JSPS KAKENHI (Grant No. JP20H02456, JP21K18860, JP22K14531, JP23H01702, and JP23K17822), JST, the establishment of university fellowships towards the creation of science technology innovation (Grant No. JPMJFS2106). We would like to thank Dr. Toshiko Mizokuro (AIST) for providing a UV/ozone cleaner and spin coater, Dr. Nobuko Fukuda (AIST) for providing a contact angle meter, and Dr. Yoshie Ishikawa (AIST) for helping us obtain the SEM images.

Notes and references

1 I. Apsite, S. Salehi and L. Ionov, *Chem. Rev.*, 2022, **122**, 1349–1415.
2 Y. Chen, J. Yang, X. Zhang, Y. Feng, H. Zeng, L. Wang and W. Feng, *Mater Horiz*, 2021, **8**, 728–757.
3 M. Ilami, H. Bagheri, R. Ahmed, E. O. Skowronek and H. Marvi, *Adv. Mater.*, 2021, **33**, 2003139.
4 H. Kim, S.-K. Ahn, D. M. Mackie, J. Kwon, S. H. Kim, C. Choi, Y. H. Moon, H. B. Lee and S. H. Ko, *Mater. Today*, 2020, **41**, 243–269.
5 R. Bo, S. Xu, Y. Yang and Y. Zhang, *Chem. Rev.*, 2023, **123**, 11137–11189.
6 J. Xiong, J. Chen and P. S. Lee, *Adv. Mater.*, 2021, **33**, 2002640.
7 D. Karnaushenko, T. Kang, V. K. Bandari, F. Zhu and O. G. Schmidt, *Adv. Mater.*, 2020, **32**, 1902994.
8 H. Zhou, S. Zhang, Z. Liu, B. Chi, J. Li and Y. Wang, *Small*, 2023, 2305805.
9 Z. Zhang, Y. Wang, Q. Wang and L. Shang, *Small*, 2022, **18**, 2105116.
10 W. Zhou, Z. Qiao, E. Nazarzadeh Zare, J. Huang, X. Zheng, X. Sun, M. Shao, H. Wang, X. Wang, D. Chen, J. Zheng, S. Fang, Y. M. Li, X. Zhang, L. Yang, P. Makvandi and A. Wu, *J. Med. Chem.*, 2020, **63**, 8003–8024.
11 G. Alici, *MRS Advances*, 2018, **3**, 1557–1568.
12 M. Rey, G. Volpe and G. Volpe, *ACS Photonics*, 2023, **10**, 1188–1201.
13 O. S. Bushuyev, M. Aizawa, A. Shishido and C. J. Barrett, *Macromol. Rapid Commun.*, 2018, **39**, 1700253.
14 M. R. A. Bhatti, A. Kernin, M. Tausif, H. Zhang, D. Papageorgiou, E. Bilotti, T. Peijs and C. W. M. Bastiaansen, *Adv. Opt. Mater.*, 2022, **10**, 2102186.
15 L. Qin, X. Liu and Y. Yu, *Adv. Opt. Mater.*, 2021, **9**, 2001743.
16 X. Pang, J.-A. Lv, C. Zhu, L. Qin and Y. Yu, *Adv. Mater.*, 2019, **31**, 1904224.
17 Y. Yang and Y. Shen, *Adv. Opt. Mater.*, 2021, **9**, 2100035.
18 B. Han, Y.-L. Zhang, Q.-D. Chen and H.-B. Sun, *Adv. Funct. Mater.*, 2018, **28**, 1802235.
19 G. Chen, J. Li, N. Li, C. Guo, P. Jin, L. Chen and Y. Peng, *Sens. Actuators B Chem.*, 2023, **383**, 133576.
20 J. Chen, J. Feng, F. Yang, R. Aleisa, Q. Zhang and Y. Yin, *Angew. Chem. Int. Ed.*, 2019, **58**, 9275–9281.
21 Q. Shi, H. Xia, P. Li, Y.-S. Wang, L. Wang, S.-X. Li, G. Wang, C. Lv, L.-G. Niu and H.-B. Sun, *Adv. Opt. Mater.*, 2017, **5**, 1700442.
22 H. Nigorikawa and H. Nakano, *Chem. Lett.*, 2022, **51**, 1150–1153.
23 H. Nakano, R. Ichikawa, H. Ukai and A. Kitano, *J. Phys. Chem. B*, 2018, **122**, 7775–7781.
24 H. Nakano and M. Suzuki, *J. Mater. Chem.*, 2012, **22**, 3702–3704.
25 W. M. Awad, D. W. Davies, D. Kitagawa, J. Mahmoud Halabi, M. B. Al-Handawi, I. Tahir, F. Tong, G. Campillo-Alvarado, A. G. Shtukenberg, T. Alkhidir, Y. Hagiwara, M. Almehairbi, L. Lan, S. Hasebe, D. P. Karothu, S. Mohamed, H. Koshima, S. Kobatake, Y. Diao, R. Chandrasekar, H. Zhang, C. C. Sun, C. Bardeen, R. O. Al-Kaysi, B. Kahr and P. Naumov, *Chem. Soc. Rev.*, 2023, **52**, 3098–3169.
26 P. Naumov, D. P. Karothu, E. Ahmed, L. Catalano, P. Commins, J. Mahmoud Halabi, M. B. Al-Handawi and L. Li, *J. Am. Chem. Soc.*, 2020, **142**, 13256–13272.
27 T. Yamaguchi and M. Ogawa, *Sci. Technol. Adv. Mater.*, 2022, **23**, 796–844.
28 D. Dattler, G. Fuks, J. Heiser, E. Moulin, A. Perrot, X. Yao and N. Giuseppone, *Chem. Rev.*, 2020, **120**, 310–433.
29 F. Tong and D.-H. Qu, *Langmuir*, 2022, **38**, 4793–4801.
30 R. O. Al-Kaysi, F. Tong, M. Al-Haidar, L. Zhu and C. J. Bardeen, *Chem. Commun.*, 2017, **53**, 2622–2625.
31 J. Mahmoud Halabi, E. Ahmed, S. Sofela and P. Naumov, *Proc. Natl. Acad. Sci. U. S. A.*, 2021, **118**, e2020604118.
32 S. Kobatake, S. Takami, H. Muto, T. Ishikawa and M. Irie, *Nature*, 2007, **446**, 778–781.
33 M. Morimoto and M. Irie, *J. Am. Chem. Soc.*, 2010, **132**, 14172–14178.
34 T. Lan and W. Chen, *Angew. Chem. Int. Ed.*, 2013, **52**, 6496–6500.
35 X. Dong, F. Tong, K. M. Hanson, R. O. Al-Kaysi, D. Kitagawa, S. Kobatake and C. J. Bardeen, *Chem. Mater.*, 2019, **31**, 1016–1022.
36 X. Dong, T. Guo, D. Kitagawa, S. Kobatake, P. Palffy-Muhoray and C. J. Bardeen, *Adv. Funct. Mater.*, 2020, **30**, 1902396.
37 F. Tong, W. Xu, T. Guo, B. F. Lui, R. C. Hayward, P. Palffy-Muhoray, R. O. Al-Kaysi and C. J. Bardeen, *J. Mater. Chem. C*, 2020, **8**, 5036–5044.
38 F. Terao, M. Morimoto and M. Irie, *Angew. Chem. Int. Ed.*, 2012, **51**, 901–904.
39 J. Lee, S. Oh, J. Pyo, J.-M. Kim and J. H. Je, *Nanoscale*, 2015, **7**, 6457–6461.
40 R. Nishimura, A. Fujimoto, N. Yasuda, M. Morimoto, T. Nagasaka, H. Sotome, S. Ito, H. Miyasaka, S. Yokojima, S. Nakamura, B. L. Feringa and K. Uchida, *Angew. Chem. Int. Ed.*, 2019, **58**, 13308–13312.
41 F. Tong, W. Xu, M. Al-Haidar, D. Kitagawa, R. O. Al-Kaysi and C. J. Bardeen, *Angew. Chem. Int. Ed.*, 2018, **57**, 7080–7084.
42 D. Kitagawa and S. Kobatake, *Chem. Commun.*, 2015, **51**, 4421–4424.
43 E. Hatano, M. Morimoto, T. Imai, K. Hyodo, A. Fujimoto, R. Nishimura, A. Sekine, N. Yasuda, S. Yokojima, S. Nakamura and K. Uchida, *Angew. Chem. Int. Ed.*, 2017, **56**, 12576–12580.

44 A. Nagai, R. Nishimura, Y. Hattori, E. Hatano, A. Fujimoto, M. Morimoto, N. Yasuda, K. Kamada, H. Sotome, H. Miyasaka, S. Yokojima, S. Nakamura and K. Uchida, *Chem. Sci.*, 2021, **12**, 11585–11592.
45 T.-Y. Xu, F. Tong, H. Xu, M.-Q. Wang, H. Tian and D.-H. Qu, *J. Am. Chem. Soc.*, 2022, **144**, 6278–6290.
46 E. Uchida, R. Azumi and Y. Norikane, *Nat. Commun.*, 2015, **6**, 7310.
47 K. Saito, M. Ohnuma and Y. Norikane, *Chem. Commun.*, 2019, **55**, 9303–9306.
48 Y. Norikane, M. Hayashino, M. Ohnuma, K. Abe, Y. Kikkawa, K. Saito, K. Manabe, K. Miyake, M. Nakano and N. Takada, *Front Chem*, 2021, **9**, 684767.
49 Y. Gong, Y. Guo, F. Ge, W. Xiong, J. Su, Y. Sun, C. Zhang, A.-M. Cao, Y. Zhang, J. Zhao and Y. Che, *Angew. Chem. Int. Ed.*, 2020, **59**, 10337–10342.
50 J. Hou, G. Long, W. Zhao, G. Zhou, D. Liu, D. J. Broer, B. L. Feringa and J. Chen, *J. Am. Chem. Soc.*, 2022, **144**, 6851–6860.
51 K. Saito, K. Ichiyanagi, S. Nozawa, R. Haruki, D. Fan, T. Kanazawa and Y. Norikane, *Adv. Mater. Interfaces*, 2023, **10**, 2202525.
52 Y. Norikane, M. Hayashino, M. Ohnuma, K. Abe, Y. Kikkawa, K. Saito, K. Manabe, K. Miyake, M. Nakano and N. Takada, *Langmuir*, 2021, **37**, 14177–14185.
53 X. Bai, X. Gou, J. Zhang, J. Liang, L. Yang, S. Wang, X. Hou and F. Chen, *Small*, 2023, **19**, 2206463.
54 M. Tenjimbayashi and K. Manabe, *Sci. Technol. Adv. Mater.*, 2022, **23**, 473–497.
55 A. Shome, A. Das, A. Borbora, M. Dhar and U. Manna, *Chem. Soc. Rev.*, 2022, **51**, 5452–5497.
56 R. J. Archer, B. Becher-Nienhaus, G. J. Dunderdale and A. Hozumi, *Adv. Funct. Mater.*, 2020, **30**, 1907772.
57 C. G. L. Furmidge, *J. Colloid Sci.* 1962, **17**, 309.
58 L. Chen, S. Huang, R. H. A. Ras and X. Tian, *Nat. Rev. Chem.,* 2023, **7**, 123–137.
59 J. V. Buddingh, A. Hozumi and G. Liu, *Prog. Polym. Sci.*, 2021, **123**, 101468.
60 J. W. Krumpfer and T. J. McCarthy, *Langmuir*, 2011, **27**, 11514–11519.
61 G. Zhang, B. Liang, Z. Zhong, Y. Huang and Z. Su, *Adv. Mater. Interfaces*, 2018, **5**, 1800646.
62 C. Urata, D. F. Cheng, B. Masheder and A. Hozumi, *RSC Adv.*, 2012, **2**, 9805.
63 C. Urata, B. Masheder, D. F. Cheng and A. Hozumi, *Langmuir*, 2012, **28**, 17681–17689.
64 Y. Zhai and T. N. Ng, *Adv. Intell. Syst.*, 2023, **5**, 2100085.
65 Q. Yang, H. Shahsavan, Z. Deng, H. Guo, H. Zhang, H. Liu, C. Zhang, A. Priimagi, X. Zhang and H. Zeng, *Adv. Funct. Mater.*, 2022, **32**, 2206939.
66 K. Manabe, K. Saito, M. Nakano, T. Ohzono and Y. Norikane, *ACS Nano*, 2022, **16**, 16353–16362.
67 Y. Norikane, M. Ohnuma, D. Kwaria, Y. Kikkawa, T. Ohzono, T. Mizokuro, K. Abe, K. Manabe and K. Saito, *Mater Horiz*, 2024, **11**, 1495–1501.
68 M. Pilz da Cunha, S. Ambergen, M. G. Debije, E. F. G. A. Homburg, J. M. J. den Toonder and A. P. H. J. Schenning, *Adv. Sci.*, 2020, **7**, 1902842.

June 24, 2024

Data Availability Statement

Title: Photo-Controllable Microcleaner: Photo-Induced Crawling Motion and Particle Transport of Azobenzene Crystals on a Liquid-Like Surface

Authors: Makoto Saikawa, Mio Ohnuma, Kengo Manabe, Koichiro Saito, Yoshihiro Kikkawa, and Yasuo Norikane*

The data that support the findings of this study are available within the article and its Supplementary Information files. Further data may be requested from the corresponding author upon reasonable request.